Vysoké učení technické v Brně

Fakulta strojního inženýrství

Ústav fyzikálního inženýrství

Ing. Tomáš Vojtek

Šíření únavových trhlin ve smykových módech II, III a II+III v prahové oblasti

Propagation of Fatigue Cracks Under Shear Loading Modes II, III and II+III in the Near-threshold Region

Zkrácená verze PhD Thesis

Studijní obor: Fyzikální a materiálové inženýrství

Školitel: prof. RNDr. Jaroslav Pokluda, CSc.

Oponenti:

Datum obhajoby:

Klíčová slova
smykové únavové trhliny, efektivní prahové hodnoty, dislokační modely růstu trhlin, vyhýbání do módu I, kvantitativní fraktografie, kovové materiály

Key Words
shear-mode fatigue cracks, effective threshold, dislocation crack growth models, mode I branching, quantitative fractography, metallic materials

Dizertační práce je uložena na oddělení vědy a výzkumu FSI VUT v Brně, Technická 2, 616 69 Brno.

ISBN 80-214-
ISSN 1213-4198

TABLE OF CONTENTS

TABLE OF CONTENTS 3

1 INTRODUCTION 5

1.2 Goals of the Work 5
1.3 Basic micromechanistic models of propagation of ideal cracks 6
1.4 Local Mode II Propagation of Remote Mode III Cracks 6
1.5 Competition Between Shear and Opening Modes 7

2 EXPERIMENTAL PROCEDURES 7

2.1 Compact-tension Shear Specimens (Mode II) 7
2.2 Cylindrical Specimens Loaded in Torsion (Mode III) 8
2.3 Cylindrical Specimens Loaded by Pure Shear (Mode II + III) 8
2.4 Investigated Materials 9
2.5 Creation of Fatigue Precracks 9

3 RESULTS AND DISCUSSIONS 9

3.1 Crack Growth Rates 9
3.2 Fractographic Analysis in Three Dimensions 11
3.3 Intrinsic Resistance to Shear-mode Crack Growth 13
3.3.2 Analytical Formulae of Intrinsic Thresholds in Modes I and II 13
3.3.3 Mode I Branching Criterion 15
3.3.4 Ratio of Modes II and III Thresholds 15
3.3.5 Important Outcomes for Materials Science and Engineering 16
3.4 Mixed mode II + III 16

4 CONCLUSIONS 17

References 18

ABSTRACT 25

1 INTRODUCTION

The history of studies of fatigue shear cracks is much shorter than that of cracks under push-pull loading. In fact, the systematic research in this field started only after 1970 [1-10]. The first works dealing with shear cracks were focused on mixed modes I + II and I + III loading and complicated fracture morphologies (factory roofs) obtained after torsion loading. Data on mode II, mode III and mixed mode II + III crack growth for various materials were preferentially reported in later works [11-17].

Precise experimental measurements are required in order to get closer to the inherent properties of materials and to compare them with the theoretical predictions. However, in the case of shear-modes cracks only a few of such data are available due to experimental problems connected to roughness-induced crack closure and the related local superposition of mode I (e.g., [12]). Recent possibilities of modelling of materials properties enable a deeper insight into the physical mechanisms of crack propagation [18,19].

One of the important mechanical properties of materials is a parameter that determines the transition from non-propagation to propagation of a cyclically loaded crack. Under small-scale yielding in metals this parameter is represented by the *threshold of the stress intensity factor range* (SIFR). In order to discuss the crack propagation phenomena near the threshold, it is helpful to divide the crack loading mechanisms into two groups – extrinsic and intrinsic ones [20,21,22]. The intrinsic (effective) mechanisms are responsible for the generation of new fracture surfaces at the crack tip, i.e., the fatigue crack propagation. The extrinsic (shielding) mechanisms occur in the surrounding of the crack tip as contacts of fracture surfaces during the cyclic loading, usually called crack closure.

1.2 GOALS OF THE WORK

The knowledge of long shear cracks behaviour improved during the last years before the start of this Ph.D. work but many aspects were still not sufficiently described or remained unclear. The most important unresolved aspects were:

- determination of effective (intrinsic) threshold values $\Delta K_{\mathrm{IIeff,th}}$, $\Delta K_{\mathrm{IIIeff,th}}$ and identification of underlying mechanisms of effective resistance to crack growth,
- experimental comparison of the near-threshold crack growth rates in modes II and III,
- quantitative description of a competition between shear and opening modes,
- appropriate description of the mixed-mode II + III crack growth data.

The main goal of this Ph.D. work is to accomplish these four points by performing and evaluating experiments with pure shear-mode crack propagation,

followed by a detailed quantitative fractography analysis in three dimensions (3D) in order to investigate the crack paths and the related local crack propagation modes. The additional goals comprise improving of a special experimental method developed and reported in [23] and to extend this method to other specimen types in order to verify the measured data and to improve mutual comparison of crack growth rates obtained for modes II and III.

The basic ideas are related to distinguishing between the macroscopic and local crack propagation mode. Crack growth under macroscopic mode is described by 'classical fracture mechanics' (linear elastic fracture mechanics) whereas 'micromechanics of fracture' focuses on microscopic level of local crack growth and the influence of microstructure of the material, which is essential for explaining the crack propagation mechanisms.

1.3 BASIC MICROMECHANISTIC MODELS OF PROPAGATION OF IDEAL CRACKS

Fatigue damage of macroscopically homogeneous and isotropic material elements ahead of the crack front of equally loaded pure mode II and mode III cracks was, for a rather long time, considered to be identical [24]. Therefore, mode II and mode III crack growth rates $(\mathrm{d}a/\mathrm{d}N)_{\mathrm{II}}$ and $(\mathrm{d}a/\mathrm{d}N)_{\mathrm{III}}$ as well as the related thresholds $\Delta K_{\mathrm{II,th}}$ and $\Delta K_{\mathrm{III,th}}$ were also expected to be equal. However, there are several experimental indications [16,25,26,27] that $\Delta K_{\mathrm{III,th}} > \Delta K_{\mathrm{II,th}}$ and $(\mathrm{d}a/\mathrm{d}N)_{\mathrm{III}} < (\mathrm{d}a/\mathrm{d}N)_{\mathrm{II}}$ which is also taken into account in numerical codes for 3D crack propagation [28,29].

Crack propagation is a consequence of cyclic plasticity at the crack tip which has a discrete nature, i.e., the explanations are based on movements of dislocations. There are two basic models dealing with different kind of possible dislocation mechanisms.

Near-threshold fatigue cracks in metallic materials propagate by a creation of new free surfaces connected to the crack front rather than by a continuous accumulation of damage inside the plastic zone. There are two most physically based models of fatigue crack growth that differ with respect to the generation of new fracture surfaces by means of a movement of discrete dislocations [30-34]. Both models, originally considered just for mode I loading, assume an ideal crack with plane crack flanks and straight crack front and predict the existence of crack-growth threshold as a consequence of the discrete nature of plasticity. Note that this is not the case of crack-growth models based on continuum mechanics [31].

1.4 LOCAL MODE II PROPAGATION OF REMOTE MODE III CRACKS

A pure mode III crack propagation is much more difficult than the mode II one. It was suggested [35] that fatigue cracks loaded in mode III can only grow by the support of local modes I and II components.

In the model reported in [20] the crack propagates by alternating step by step mode II growth (under the resolved shear stress component $\tau_{II,d}$) of the diversely oriented crack front segments. This leads to gradual smoothing of the crack front and may decelerate the remote mode III crack growth. After a certain number of cycles, the shape of the crack front looks similar to a mode III-like crack propagation.

The second model considers even a microscopically straight crack front but the assistance of secondary phase particles is needed here. Dislocation pile-ups are gradually generated at the particle-matrix interfaces and eventually produce microcracks perpendicularly oriented to the main crack front. These cracks can then extend under the local mode II along the crack front.

1.5 COMPETITION BETWEEN SHEAR AND OPENING MODES

Mode II and mode III fracture morphologies considerably differ particularly in the near-threshold region [20]. The change in the crack growth direction is related to a competition between shear and opening loading modes that can lead to mode I branching. Some simple concepts for the description of the mode I branching condition for mode II cracks were also proposed [9,10] but their verification is difficult due to a lack of reliable effective values of ΔK_{IIeff}. Small semi-elliptical shear cracks, initially growing coplanar with the precrack in remote modes II and III, are often observed to form mode I branches – see Fig. 1.

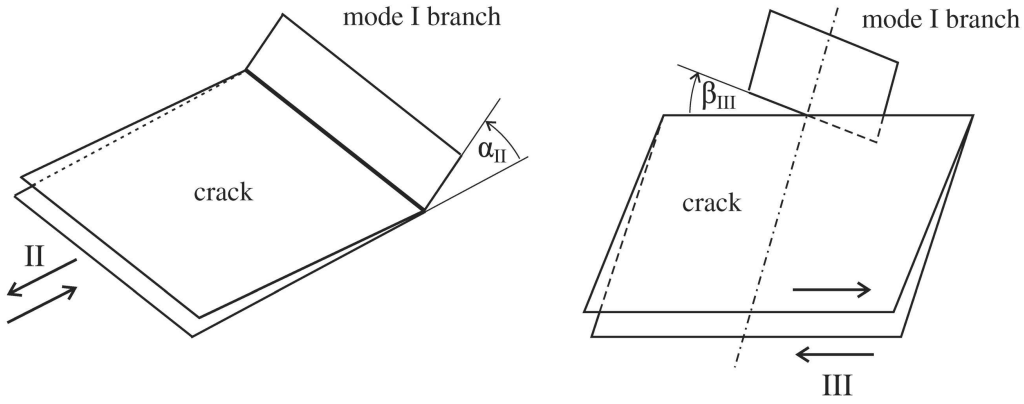

Fig. 1. Schematic illustration of deflected and twisted cracks forming mode I branches under mode II and mode III loading, respectively.

2 EXPERIMENTAL PROCEDURES

2.1 COMPACT-TENSION SHEAR SPECIMENS (MODE II)

A standard device for mode I + II testing was used for pure mode II loading of compact tension-shear (CTS) specimens. The SIFs were calculated using numerically determined formulas for the CTS specimens [36].

2.2 CYLINDRICAL SPECIMENS LOADED IN TORSION (MODE III)

Pure mode III experiments were conducted by means of a special device transforming tensile or compressive force to torsion loading of a cracked cylindrical specimen with the same geometry as in the pure shear experiment (see hereafter). The specimens were fixed into this device by ring clamping elements and loaded by cyclic torque T. The SIFs were calculated using the asymptotic relationship published in [37].

2.3 CYLINDRICAL SPECIMENS LOADED BY PURE SHEAR (MODE II + III)

To load a single specimen simultaneously by remote mode II, mode III and mixed mode II + III, a special testing device was utilized [16,38]. The device transforms tensile forces to a simple-shear loading of circumferentially notched cylindrical bars with the inner diameter d = 12 mm and the outer diameter D = 25 mm (Fig. 2). At the exact central point of the bar the bending moment was zero when considering ideal testing conditions and, therefore, no superposition of mode I was present. The circumferential crack was subjected to cyclic shear loading that resulted in various combinations of modes II and III (Fig. 2c) as a function of the polar angle φ. At the top and the bottom of the circular cross-section the crack was loaded in a pure mode II, on the left and right in a pure mode III and, in between, a mixed-mode II + III loading was applied.

The precracks started at the notch of the depth l_{n1} = 6.5 mm and reached the length l_o. The lengths l_o and the shear-crack length l_s were measured in SEM images of fracture surfaces. The dependences of modes II and III SIFs (Eq. 12) on both the fatigue crack length $l_o + l_s/2$ and the angle φ were calculated using FEM [39].

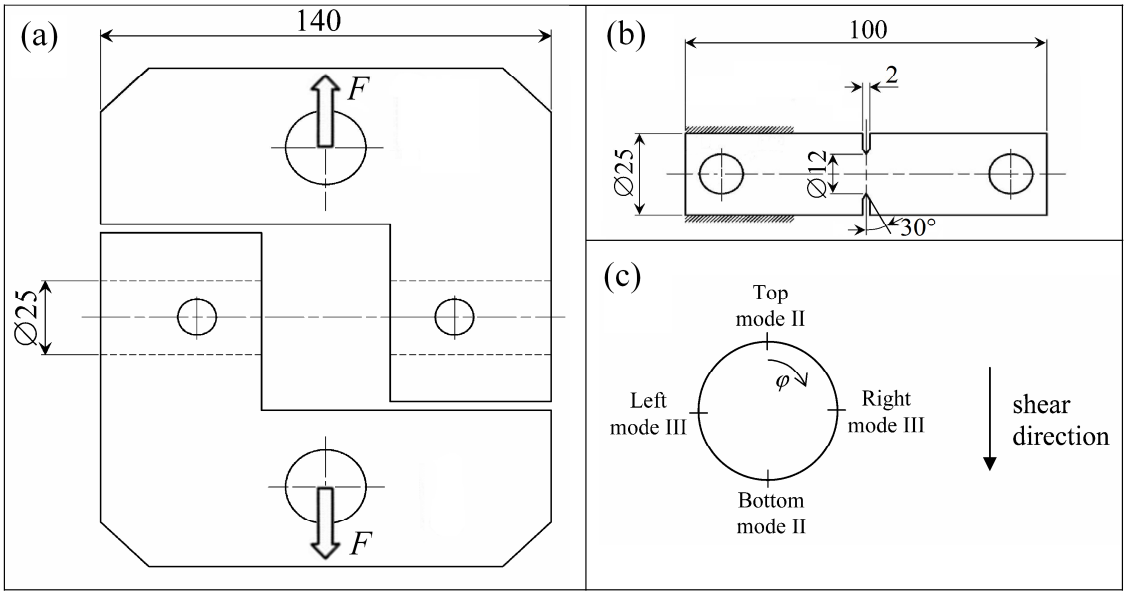

Fig. 2. Scheme of the experiment with cylindrical specimens loaded in pure shear: (a) loading device; (b) pure shear specimen; (c) specimen cross section with the corresponding loading modes.

2.4 INVESTIGATED MATERIALS

Experiments were done with four different single-phase metallic materials of various crystal lattices. The first material was ARMCO iron, a representative of body-centred cubic (bcc) metals. It is a nearly pure polycrystalline ferrite. It was received in a cold-rolled state and after annealing, it had the yield strength $\sigma_y \approx 150$ MPa and the mean grain size $d_m \approx 110$ μm.

The commercially pure polycrystalline α-titanium (Grade 2) was investigated as a representative of metals with the hexagonal close-packed (hcp) lattice. Two different microstructures of this material were prepared by applying annealing temperatures of 850 °C ($\sigma_y \approx 180$ MPa, $d_m \approx 50$ μm) and 950 °C ($\sigma_y \approx 230$ MPa, $d_m \approx 1$ μm). The latter microstructure, (denoted Ti-needles), contained fine needle-shaped grains of a preferential crystallographic orientation with the mean spacing of about 10 μm.

Two materials with the face-centered cubic (fcc) lattice were also selected. The first was a cold-rolled austenitic steel X5CrNi18-10 with the yield strength after annealing $\sigma_y \approx 230$ MPa. The austenitic steel has a low stacking fault energy (SFE) and, therefore, another fcc material with a high SFE was selected – commercially pure nickel 201 (99.5% Ni) that had the yield strength $\sigma_y \approx 140$ MPa after annealing.

2.5 CREATION OF FATIGUE PRECRACKS

Fatigue precracks were generated under pure cyclic compression at the notch root of all specimens. In this way, the crack closure effects could be substantially suppressed at the onset of the experiment. After pre-fatigue loading, the specimens were annealed to recrystallize in order to avoid any effect of pre-fatigue and hardening of the material, i.e. to eliminate residual stresses and plastic zone at the crack front. It also caused a further smoothening of the precrack facets resulting in even more eliminated roughness-induced crack closure. Annealing and cooling down of the specimens were done in vacuum to avoid generation of oxide layer at the precrack surfaces and the related oxide-induced crack closure effect.

3 RESULTS AND DISCUSSIONS

3.1 CRACK GROWTH RATES

The near-threshold crack growth rate data obtained for all investigated materials were plotted as diagrams $\Delta a/\Delta N$ vs. ΔK_{II} in Fig. 3. The values $\Delta a/\Delta N$ were determined as averaged crack growth rates of the shear-mode cracks during $\Delta N = 10^5$ cycles when the crack growth rate was gradually decreasing due to an increasing friction-induced crack closure. In all experiments, the related ratio $\Delta a/a \approx 0.01$ was very small and the corresponding changes of ΔK during the shear-mode crack growth could, therefore, be considered to be negligible.

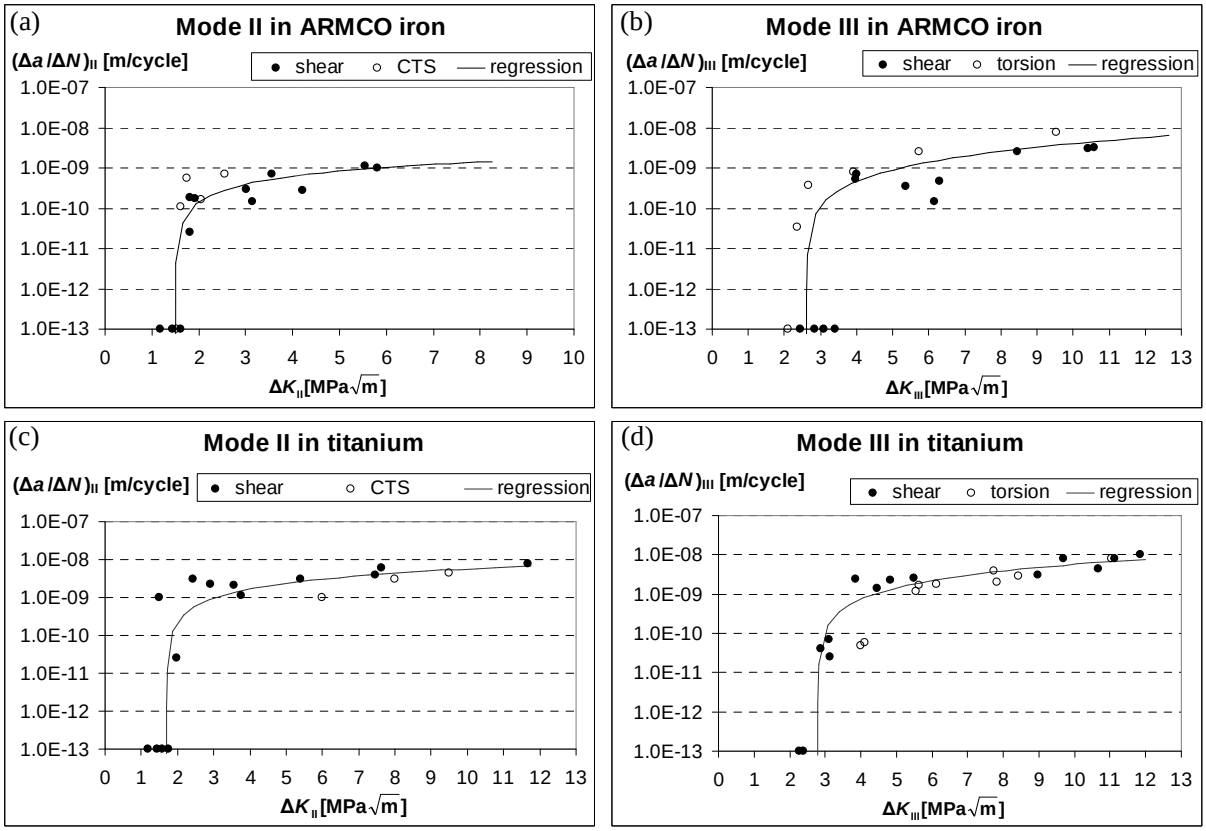

Fig. 3. Mean crack growth rate data of remote modes II and III loaded crackrs for (a), (b) ARMCO iron; (c), (d) for α-titanium. The threshold values $\Delta K_{II,th}$ and $\Delta K_{III,th}$ for $\Delta a/\Delta N = 10^{-13}$ m/cycle are very close to the effective ones. The calculated ΔK_{II} and ΔK_{III} are global K values which do not take into account crack branching. Full circles – pure shear specimens, hollow circles – CTS specimens in mode II, torsion specimens in mode III.

These crack growth data were fitted using the equation $\Delta a/\Delta N = A(\Delta K^n - \Delta K_{th}^n)$ suitable for the near-threshold region [40]. The data corresponding to the absence of crack growth (below the threshold) are assigned to $\Delta a/\Delta N = 10^{-13}$ m/cycle. With regard to an expected high scatter near the threshold, the data obtained using single-shear and CTS specimens are in a good agreement and the effective threshold values, $\Delta K_{IIeff,th}$, could be determined with a reasonable precision. These values are displayed in Table 2 for all investigated materials.

In the ARMCO iron the crack growth rates are similar in both modes II and III, while in austenitic steel the crack growth rates are different in modes II and III. This is caused by the difference in levels of roughness-induced crack closure. In ARMCO iron small deviation of crack growth directions cause the same level of friction in modes II and III. In austenitic steel the branches to local mode I cause that a highly deflected crack in the remote mode II is open and friction is reduced, whereas the factory-roof morphology in the remote mode III cause clamping of fracture surface and a high level of friction. The higher the tendency to deviate/twist to local mode I, the higher retardation of remote mode III cracks compared to those of remote mode II. ARMCO iron and austenitic steel exhibit the highest level of this effect. In a lower extent it can also be seen in nickel and titanium.

3.2 FRACTOGRAPHIC ANALYSIS IN THREE DIMENSIONS

Micrographs of fracture surfaces from the experiments are presented in Fig. 4 and Fig. 5. Three crack path regions can be distinguished on the fracture morphology of the four investigated materials. They are marked by white lines: a precrack emanating from the notch, the shear crack and the final fracture (brittle or fatigue fracture in mode I).

After the experiments, fracture surfaces of all specimens were examined by SEM and their morphologies were recontructed in 3D using stereophotogrammetry in SEM in order to identify local crack-path deviations of shear cracks from the coplanar crack growth. The computed height profiles running parallel to the direction of applied shear stress are in Fig. 4 – Fig. 5. The vertical cutting planes that define the profiles are denoted by long white arrows. The coordinate l passes along the line from the left to the right or from the top to the bottom and the topological data are determined by the vertical coordinate z. These profiles were used for measurement of angles corresponding to the crack deflection or twisting from the crack (the maximum shear stress plane).

The profiles running parallel to shear provided deflection angles α_{II} in mode II and twisting angles β_{III} in mode III. The angles indicate the levels of deflection and twisting of crack fronts, determining the amount of local mode I support to in-plane shear crack propagation. Mean values and standard deviations of all angles are summarized separately for each of the two specimen types in Table 1.

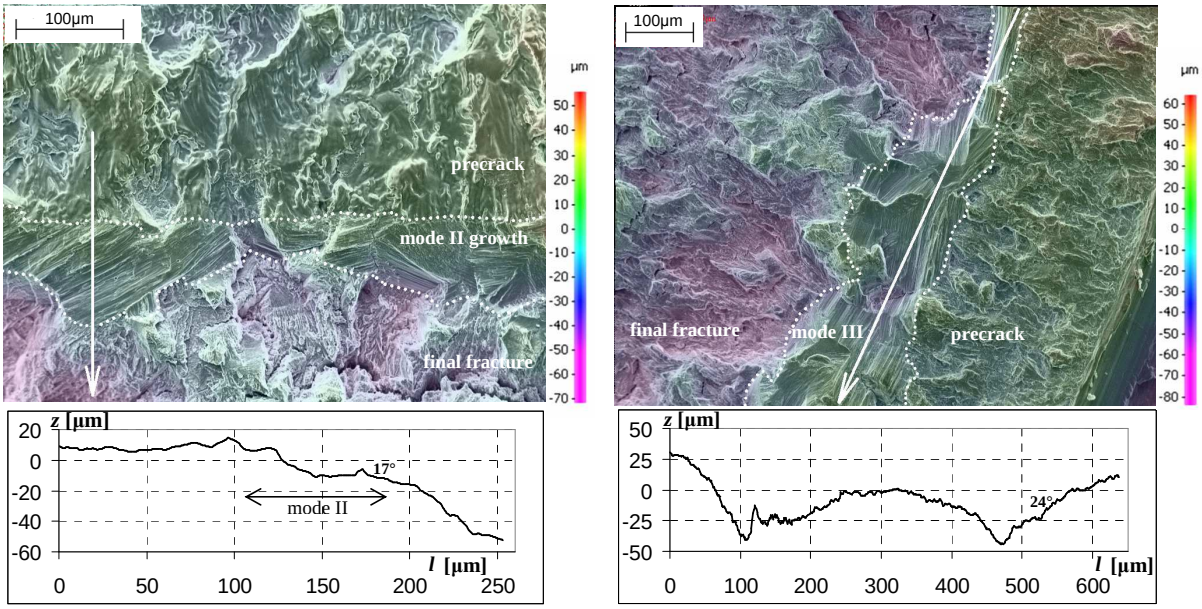

Fig. 4 Examples of fracture morphology and profiles along the indicated arrows for mode II and mode III in ARMCO iron. The heights in three dimensions can be assessed according to the colour codes.

In the ARMCO iron, both mode II and mode III faceted fracture surfaces suggest an influence of crystallography on the crack growth. Diversely oriented fibrous

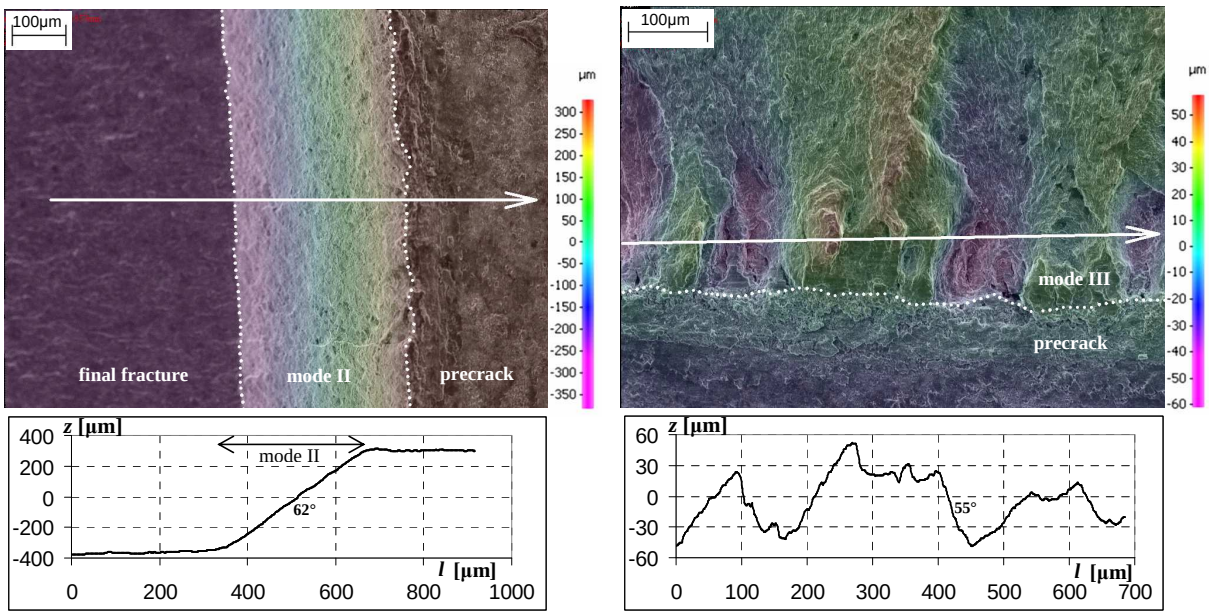

Fig. 5 Examples of fracture morphology and profiles along the indicated arrows for mode II and mode III in austenitic steel. The heights in three dimensions can be assessed according to the colour codes.

patterns with spatially random orientation may be confined to facets within individual grains. These fibrous marks highlight the positions of local crack front elements inside individual facets, which are mostly not parallel to the applied shear direction. The local crack propagation directions possess a noticeable mode II component parallel with the direction of applied shear stress. This corresponds to the model of local mode-II controlled micromechanism. The crack propagates in local mixed-mode I + II + III directions but the mode II crack growth was predominant in both remote modes II and III loading cases. The fracture surfaces in the ARMCO iron are rather smooth with small relatively small mean angles (≈ 19°) of both deflection and twisting angles in all directions, which indicates a nearly coplanar crack growth.

Table 1. Mean deflection angles [°] of mode II cracks and twisting angles [°] of mode III cracks.

				specimen	
				shear	CTS
mode II	α_{II} [°]	deflection	ARMCO iron	18 ± 17	19 ± 8
			austenitic steel	66 ± 4	67 ± 5
			Ti	23 ± 19	56 ± 12
			Ti (needles)	43 ± 23	33 ± 30
			Ni	54 ± 22	50 ± 25
mode III	β_{III} [°]	twist	ARMCO iron	19 ± 13	13 ± 10
			austenitic steel	33 ± 23	45 ± 8
			Ti	29 ± 21	38 ± 21
			Ti-needles		41 ± 19
			Ni	38 ± 22	34 ± 21

A clear influence of crystallography was also detected on the fracture surfaces of both titanium grades but the angles α_{II} and β_{III} were found to be considerably higher. Even higher angles α_{II} and β_{III} were identified in nickel where the deflection of some facets was already close to the theoretical value of 70.5° of pure mode I branches of the remote II cracks and 45° of the remote mode III ones [41]. Nevertheless, the crystallographical morphology was still present at the whole fracture surface of both mode II and mode III loaded nickel specimens. In the austenitic steel, all the deflection and twist angles α_{II} and β_{III} approached the theoretical values for pure mode I branches. The fracture surfaces are locally rather smooth with no sign of crystallography influence and the morphology was very similar to that observed under mode I loading [38].

3.3 INTRINSIC RESISTANCE TO SHEAR-MODE CRACK GROWTH

Effective thresholds $\Delta K_{IIeff,th}$ and $\Delta K_{IIIeff,th}$ for ARMCO iron, austenitic steel, titanium and nickel are displayed in Table 2. First, the question arises if the values of $\Delta K_{IIeff,th}$ and $\Delta K_{IIIeff,th}$ are really the effective ones. This can be assessed by comparison with results of atomistic models for cracked iron single crystal [42,43]. These models give the averaged value $k_{IIe} \approx 0.75$ MPa·m$^{1/2}$ for generation of first dislocation during monotonic loading. Assuming the factor of 1.3 – 1.5 to reach the cyclic threshold [31] it gives $\Delta K_{IIeff,th} \approx$ 1.0 – 1.2 MPa·m$^{1/2}$. This is in good agreement with the result of 1.5 MPa·m$^{1/2}$ for ARMCO iron that is expected to be somewhat higher than that for the single crystal due to incompatible geometrical crack/slip conditions for the dislocation emission in individual grains along the crack front.

Table 2. Measured effective thresholds $\Delta K_{IIeff,th}$ and $\Delta K_{IIIeff,th}$

Material	$\Delta K_{IIth,eff}$ [MPa·m$^{1/2}$]	$\Delta K_{IIIth,eff}$ [MPa·m$^{1/2}$]
ARMCO iron	1.5	2.6
Titanium	1.7	2.8
Austenitic steel	2.5	4.2
Nickel	2.9	4.3

3.3.2 Analytical Formulae of Intrinsic Thresholds in Modes I and II

The threshold data can be discussed from the point of view of the underlying physical principles. Liaw et al. [44] predicted that the effective mode I thresholds in metallic materials should be proportional to the Young modulus *E*. This was confirmed and further refined by the discrete dislocation models [31] which predicted the proportionality

$$\Delta k_{Ie} \approx q_I E \sqrt{b} \qquad (1)$$

and, in the case of mode II cracks

$$\Delta k_{\mathrm{IIe}} \approx q_{\mathrm{II}} G\sqrt{b}\,, \tag{2}$$

where G is the shear modulus, b is the magnitude of Burgers vector and q_{I} and q_{II} are dimensionless coefficients. Values E, G and b for investigated metals were taken into account.

The simple deformation-based models consider a coplanar shear-mode crack propagation that was observed in the ARMCO iron only. In other metals the crack propagated along significantly deflected planes (see Table 1). This difference can be attributed to a much higher number of slip systems available for shear crack propagation in the bcc lattice when compared to both fcc and hcp ones. In the bcc structure, a dense spatial set of possible slip systems <111> {110} and <111> {112} is available for dislocation emission and slip. This set consists of slip planes mutually exhibiting as much as nine different angles in the range of 0 – 90 degrees. Therefore, there is a high probability to find slip planes in grains adjacent to the precrack front and exhibiting the Schmid factor comparable to that of the precrack plane of maximum shear stress. Consequently, the crack can easily propagate along such slip planes by only slight deviations with respect to the precrack plane. On the other hand, the possible slip systems <110> {111} in fcc structures of nickel and austenitic steel form a very thin set of planes exhibiting only one angle between 0 – 90 degrees. In the hcp lattice of titanium, similarly, the plastic deformation in the direction of c -axis cannot be ensured by easy slips in basal and prismatic systems. As a consequence, a significantly lower averaged local $\Delta k_{\mathrm{IIeff,d}}$ on deflected slip planes raises the $\Delta K_{\mathrm{IIeff,th}}$ value in fcc and hcp metals. This corresponds well to high deflection angles α_{IIm} of fracture facets measured for these materials (see Table 1).

The Eqs. (1) and (2) can be modified to the following formulas for effective mode I and II thresholds:

$$\Delta K_{\mathrm{Ieff,th}} = q_{\mathrm{I}} E\sqrt{b}\,, \tag{1a}$$

$$\Delta K_{\mathrm{IIeff,th}} = \frac{q_{\mathrm{II}}}{n_{\alpha}} G\sqrt{b}\,, \tag{2a}$$

where $n_{\alpha} = \frac{1}{2}\cos\frac{\alpha_{\mathrm{IIm}}}{2}(3\cos\alpha_{\mathrm{IIm}} - 1)$ [45]. This Eq. (2a) can be used for a rough prediction of $\Delta K_{\mathrm{IIeff,th}}$ for metallic materials when assuming $n_{\alpha,\mathrm{bcc}} \approx 0.9$, $n_{\alpha,\mathrm{hcp}} \approx 0.6$ and $n_{\alpha,\mathrm{fcc}} \approx 0.4$ for bcc, hcp and fcc metals, respectively. For fcc metals with a very low stacking fault energy, however, Eq. (1a) should be applied instead of Eq. (2a).

Table 3. Comparison of experimental and theoretical effective thresholds in modes I and II.

material	$\Delta K_{\mathrm{Ieff,th}}$ [MPa·m$^{1/2}$]		$\Delta K_{\mathrm{IIeff,th}}$ [MPa·m$^{1/2}$]	
	experiment	Eq. (1a)	experiment	Eq. (2a)
ARMCO iron	2.7[a)]	2.5	1.5	1.4
Titanium	2.0[b)]	2.0	1.7	1.7
Nickel		2.3	2.9	3.1
Austenitic steel	2.3[c)]	2.5	2.5	2.5[d)]

[a)] [46], [b)] [47,48], [c)] [49], [d)] Eq.(1a)

3.3.3 Mode I Branching Criterion

When knowing the effective values $\Delta K_{\mathrm{IIeff,th}}$, one can check the validity of the simple branching (bifurcation) criterion $\Delta k_{\mathrm{Id}} = 1.15\,\Delta K_{\mathrm{IIeff,th}} \geq \Delta K_{\mathrm{Ieff,th}}$ at the crack growth thresholds of all investigated materials. This is presented in Table 4. When inserting Eqs. (1a) and (2a) into the criterion, $1.15\,\Delta K_{\mathrm{IIeff,th}} = \Delta K_{\mathrm{Ieff,th}}$, the transition branching angle $\alpha_{\mathrm{IIts}} \approx 40°$ can be determined as a value practically independent of a material. Indeed, one gradually obtains ($\nu \approx 0.3$) [45]:

$$n_\alpha = 1.15\frac{4G}{3E} \approx \frac{0.77}{1+\nu} \approx 0.6 = \frac{1}{2}\cos\frac{\alpha_{\mathrm{IIts}}}{2}(3\cos\alpha_{\mathrm{IIts}} - 1) \;\rightarrow\; \alpha_{\mathrm{IIts}} \approx 40^{\mathrm{o}} \tag{26}$$

Table 4. Fulfilment of the branching criterion $\Delta k_{\mathrm{Id}} \geq \Delta K_{\mathrm{Ieff,th}}$

Material	Branching criterion [MPa·m$^{1/2}$]
ARMCO iron	1.7 < 2.7
Titanium	2.0 ≈ 2.0
Nickel	3.3 > 2.3
Austenitic steel	2.9 > 2.3

With respect to Table 4, obviously, the value $\alpha_{\mathrm{IIts}} \approx 40°$ and the related mode mixity $\Delta k_{\mathrm{IIeff,d}}/\Delta k_{\mathrm{Ieff,d}} = 0.67$ according to Eq. (19) well correspond to respective $\alpha_{\mathrm{IIm}} = 39°$ and $\Delta k_{\mathrm{IIeff,d}}/\Delta k_{\mathrm{Ieff,d}} = 0.70$ as measured for titanium. Although the branching condition in nickel is fulfilled, the global character of the morphology is still of a crystallographic shear dominance.

3.3.4 Ratio of Modes II and III Thresholds

The k_{IIIe} values for the coplanar emission of screw dislocations at the mode III crack front (see, for example [43]) were estimated to be somewhat smaller than those of k_{IIe}, which would not fit the measured ratio $\Delta K_{\mathrm{IIIeff,th}}/\Delta K_{\mathrm{IIeff,th}} \approx 1.7$ for investigated materials at all. If one supposes that only the local mode II segments propagate under global mode III loading then the local mode II stress components at the microtortuous crack front should only be taken into account. Assuming that the mean deviation angle of the in-plane ledges of the precrack front is 30°, the ratio of

the local mode II and mode III shear stress is $\tau_{II,local}/\tau_{III,local}$ = 0.5 as follows from a geometrical separation of the local shear stresses [35] and, consequently, the ratio $\Delta K_{IIIeff,th}/\Delta K_{IIeff,th}$ should be about 2. However, the in-plane angle of 30°is rather an upper limit of the precrack tortuosity. Therefore, it seems that also mechanisms other than the local mode II displacements partially contribute to mode III crack growth as, e.g., the accumulative damage mechanism inside the cyclic plastic zone.

3.3.5 Important Outcomes for Materials Science and Engineering

At the threshold loading level (R = 0.1), the extent of the cyclic plastic zone, R_p, at the precrack tip is less than (or comparable to) the characteristic microstructural distance in all the investigated materials. This means that the influence of microstructural barriers does not play any important role and the main factors controlling the intrinsic shear-mode thresholds are only related to matrix (lattice) characteristics G, b and α_{IIm} that explicitly appear in Eq. (2a). A high intrinsic shear-mode threshold is, therefore, ensured by a high shear modulus G (high strength of interatomic bonds), a long Burgers vector (small manoeuvrability of dislocations) and a high mean deflection angle α_{IIm} (small number of available slip systems).

Height of the crack-wake asperities, which depends on the level of local mode I branching, determines the difference between crack growth rates in modes II and III. In material with relatively plain fracture surfaces (emission of dislocations from the crack tip is a dominant mechanism) crack growth rates in modes II and III are nearly comparable. On the other hand, crack growth rates are much higher for mode III than those of mode II in materials where factory-roof crack flanks are generated. Considering the relationship $\Delta K_{applied} = \Delta K_{effective} + \Delta K_{closure}$, effective thresholds, which can be obtained by the experimental procedure presented in this work, enable predicting of the closure component:

$$\Delta K_{closure} = \Delta K_{applied} - \Delta K_{effective}.$$

3.4 MIXED MODE II + III

In order to describe the mixed-mode II + III crack propagation, there is effort to express the data in terms of an equivalent stress intensity range (ΔK_{eq}). The experimentally obtained mixed-mode crack growth rate data can were described by an equivalent SIFR $\Delta K_{eq} = \sqrt{\Delta K_{II}^{\ 2} + \lambda \Delta K_{III}^{\ 2}}$. The coefficient λ decides about the weights of contributions of mode II and III components. The results showed that the data were best fitted when $\lambda \approx 1.1$. This value is less than $1/(1 - \nu)$ which means that, in the near-threshold regime, the mode III component of the crack driving force was slightly less efficient than that of the mode II.

4 CONCLUSIONS

Experiments were done in the near-threshold region of the shear-mode crack growth in metallic materials and brought new data on effective crack growth thresholds for ARMCO iron, α-titanium, nickel and austenitic steel. Experimental data were obtained for two types of specimens for each of loading modes II and III. Observations of fracture surfaces in three dimensions were done by means of stereophotogrammetry in SEM.

Analysis of crack deviation angles revealed that in the ARMCO iron the cracks deflected and twisted randomly in all directions by a small angle ~ 20° and that the crack propagated along the maximum shear plane. The facets in the ARMCO iron indicated a significant influence of crystallography. In austenitic steel the high deflection and twisting angles corresponded to local mode I branching in both remote mode II and remote mode III. No crystallographic influence was observed in austenitic steel. According to these observations, the model of shielding dislocations can be attributed to crack growth in the ARMCO iron and the model of absorption of antishielding dislocations can be applied on crack growth in the austenitic steel.

In all investigated materials, the effective thresholds $\Delta K_{\mathrm{IIeff,th}}$ under the remote mode II loading were found to be about 1.7 times lower than the thresholds $\Delta K_{\mathrm{IIIeff,th}}$ under the remote mode III loading.

Effective thresholds under mode I and mode II loading of investigated materials follow the relationships $\Delta K_{\mathrm{Ieff,th}} = 3E\sqrt{b}/4$ and $\Delta K_{\mathrm{IIeff,th}} = G\sqrt{b}/n_{\alpha}$, respectively, where E and G are the respective Young's and shear moduli, b is the magnitude of Burgers vector and n_{α} is a function of mean deflection angle α_{IIm}: $n_{\alpha,\mathrm{bcc}} \approx 0.9$, $n_{\alpha,\mathrm{hcp}} \approx 0.6$ and $n_{\alpha,\mathrm{fcc}} \approx 0.4$ can roughly be assumed for bcc, hcp and fcc metals, respectively. Consequently, the intrinsic resistance to shear-mode crack growth is predetermined by strength of interatomic bonds (G), manoeuvrability of dislocations (b) and the number of slip systems in the lattice (n_{α}).

The simple criterion $1.15\Delta K_{\mathrm{IIeff,th}} \geq \Delta K_{\mathrm{Ieff,th}}$ for mode I branching well reflects a transition from the shear-mode to the opening-mode controlled crack propagation. The associated deflection angle $\alpha_{\mathrm{IIts}} \approx 40°$ practically does not depend on a material.

Finally, it should be emphasized that the level of friction-induced closure component is usually several times higher than the effective one in the near-threshold region. Therefore, the shear-mode crack growth behaviour is predominantly determined by extrinsic factors and the experimental work to find the intrinsic resistance to shear-mode crack growth is of a rather subtle nature.

Verification of the results for other single-phase materials (Nb, Zr) and two-phase materials (ferritic-pearlitic steel, pure pearlitic steel, Ti-6Al-4V alloy) is planned to be done in the future.

REFERENCES

[1] LAWN, B. R.; WILSHAW, T. R. *Fracture of Solids*. Cambridge: Cambridge University Press, 1975.

[2] OTSUKA, A; MORI, K; MYIATI, T. The condition of fatigue crack growth in mixed mode condition. *Engineering Fracture Mechanics*, 1975, vol. 7, pp. 429-439.

[3] SWEDLOW, J. L. Criteria for growth of the angled cracks. *Cracks and Fracture*, ASTM STP 601, 1976, West Conshohocken: ASTM, pp. 506-521.

[4] HOURLIER, F.; McLEAN, D.; PINEAU, A. Fatigue crack growth behaviour of Ti-5Al-2-5Sn alloy under complex stress (mode I + steady mode III). *Metals Technology*, 1978, vol. 5, pp. 154-158.

[5] HOURLIER, F.; PINEAU, A. Propagation of fatigue cracks under polymodal loading. *Fatigue & Fracture of Engineering Materials & Structures*, 1982, vol. 5, pp. 287-302.

[6] TSCHEGG, E. K. The influence of the static load mode I and R ratio on mode III fatigue crack growth behaviour in mild steel. *Materials Science and Engineering*, 1982, vol. 54, pp. 127-136.

[7] TSCHEGG, E. K.; RITCHIE, R. O.; McCLINTOCK, F. A. On the influence of rubbing fracture surfaces on fatigue crack propagation in mode III. *International Journal of Fatigue*, 1983, vol. 5, pp. 29-35.

[8] TSCHEGG, E. K. Sliding mode crack closure and mode III fatigue crack growth in mild steel. *Acta Metallurgica*, 1984, vol. 31, pp. 1323-1330.

[9] POOK, L. P. The fatigue crack direction and threshold behaviour of mild steel under mixed mode I and III loading. *International Journal of Fatigue*, 1985, vol. 7, pp. 21-30.

[10] BROWN, M. W.; HAY, E.; MILLER, K. J. Fatigue at notches subjected to reversed torsion and static axial loads. *Fatigue & Fracture of Engineering Materials & Structures*, 1985, vol. 8, pp. 243-258.

[11] OTSUKA, A.; MORI, K.; TOGHO, K. Mode II fatigue crack growth in aluminium alloys. *Current Japanese Materials Research*, 1987, vol. 1, pp. 163-185.

[12] TSCHEGG, E. K.; STANZL, S. E. The significance of sliding mode crack closure on mode III fatigue crack growth. *Basic questions in fatigue*, ASTM STP 924, vol. 1, West Conshohocken: ASTM, 1988, pp. 214-232.

[13] HELLIER, A. K.; McGIRR, M. B.; CORDEROY, D. J. H. A finite element and fatigue threshold study of shelling in heavy haul rails. *Wear*, 1991, vol. 144, pp. 289-306.

[14] DOQUET, V.; POMMIER, S. Fatigue crack growth under non-proportional mixed-mode loading in ferritic-pearlitic steel. *Fatigue & Fracture of Engineering Materials & Structures*, 2004, vol. 27, pp. 1051-1060.

[15] VAZIRI, A.; NAYEB-HASHEMI, H. The effect of crack surface interaction on the stress intensity factor in Mode III crack growth in round shafts. *Engineering Fracture Mechanics*, 2005, vol. 72, pp. 617-629.

[16] POKLUDA, J; TRATTNIG, G.; MARTINSCHITZ, C.; PIPPAN, R. Straightforward comparison of fatigue crack growth under modes II and III. *International Journal of Fatigue*, 2008, vol. 30, pp. 1498-1506.

[17] DOQUET, V.; BUI, Q. H.; BERTOLINO G.; MERHY, E.; ALVES, L. 3D shear-mode fatigue crack growth in maraging steel and Ti-6Al-4V. *International Journal of Fracture*, 2010, vol. 165, pp. 61-76.

[18] UHNÁKOVÁ, A.; POKLUDA, J.; MACHOVÁ, A.; HORA, P. 3D atomistic simulation of fatigue behaviour of cracked single crystal of bcc iron loaded in mode III. *International Journal of Fatigue*, 2011, vol. 33, pp. 1564-1573.

[19] UHNÁKOVÁ, A.; POKLUDA, J.; MACHOVÁ, A.; HORA, P. 3D atomistic simulation of fatigue behavior of a ductile crack in bcc iron loaded in mode II. *Computational Material Science*, 2012, vol. 61, pp. 12-19.

[20] POKLUDA, J.; ŠANDERA, P. *Micromechanisms of Fracture and Fatigue*. London: Springer, 2010. 295 p. ISBN 978-1-84996-265-0.

[21] RITCHIE, R. O. Mechanisms of fatigue crack propagation in metals, ceramics and composites: Role of crack tip shielding. *Materials Science and Engineering: A*, 1988, vol. 103, pp. 15-28.

[22] SURESH, S. *Fatigue of Materials.* Cambridge: Cambridge University Press, 1998, 704 p.

[23] HOLÁŇ, L.; POKLUDA, J.; SLÁMEČKA, K. Local Aspects of Shear-mode Crack Propagation in Austenitic Steel. *Chemické Listy*, 2010, vol. 104, pp. 314-317.

[24] MURAKAMI, Y.; KUSUMOTO, R.; TAKAHASHI, K. Growth mechanism and threshold of mode II and mode III fatigue crack. *Fracture mechanics beyond 2000 (ECF 14)*, vol. II. Sheffield: EMAS, 2002, pp. 493-500.

[25] RITCHIE, R. O.; McCLINTOCK, F. A.; NAYEB-HASHEMI, H.; RITTER, M. A. Mode III fatigue crack propagation in low alloy steel. *Metallurgical Transactions A*, 1982, vol. 13, pp. 101-110.

[26] NAYEB-HASHEMI, H.; McCLINTOCK, F. A.; RITCHIE, R. O. Micro-mechanical modelling of mode III fatigue crack growth in rotor steels. *International Journal of Fracture*, 1983, vol. 23, pp. 163-185.

[27] HELLIER, A. K.; McGIRR, M. B.; CORDEROY, D. J. H.; KUTAJCZYK, L. A. Fatigue of head hardened rail steel under mode III loading. *International Journal of Fracture*, 1990, vol. 42, pp. R19-R23.

[28] JAMES, M.; HERMAN, D. J.; SCOTT, F. Crack Growth Rate Stress Intensity Factor Corrections for Out-of-Plane Crack Growth. In *Fatigue and Fracture Mechanics*. Ed. S. R. DANIEWITZ, J. C. NEWMAN, K. H. SCHWALBE, West Conshohocken: ASTM, 2003.

[29] SCHÖLLMANN, M.; FULLAND, M.; RICHARD, H. A. Development of a new software for adaptive crack growth simulations in 3D structures. *Engineering Fracture Mechanics*, 2003, vol. 70, pp. 249-268.

[30] PIPPAN, R. Dislocation emission and fatigue crack-growth threshold. *Acta Metallurgica et Materialia*, 1991, vol. 39, pp. 255-262.

[31] RIEMELMOSER, F. O.; GUMBSCH, P.; PIPPAN, R. Dislocation modelling of fatigue cracks: An overview. *Materials Transactions, JIM*, 2001, vol. 42, pp. 2-13.

[32] PIPPAN, R.; RIEMELMOSER, F. O.; WEINHANDL, H.; KREUZER, H. Plasticity-induced crack closure under plane-strain conditions in the near-threshold regime. *Philosophical Magazine A*, 2002, vol. 82, pp. 3299-3309.

[33] DESHPANDE, V. S.; NEEDLEMAN, A; VAN DER GIESSEN, E. A discrete dislocation analysis of near-threshold fatigue crack growth. *Acta Materialia*, 2001, vol. 49, pp. 3189-3203.

[34] VAN DER GIESSEN, E; DESHPANDE, V. S.; CLEVERINGA, H. H. M.; NEEDLEMAN, A. Discrete dislocation plasticity and crack tip fields in single crystals. *Journal of the Mechanics and Physics of Solids*, 2001, vol. 49, pp. 2133-2153.

[35] POKLUDA, J.; PIPPAN, R. Can a pure mode III fatigue loading contribute to crack propagation in metallic materials? *Fatigue & Fracture of Engineering Materials & Structures*, 2005, vol. 28, pp. 179-186.

[36] PLANK, R.; KUHN, G. Fatigue crack propagation under non-proportional mixed mode loading. *Engineering Fracture Mechanics*, 1999, vol. 62, pp. 203-229.

[37] BENTHEM, J. P.; KOITER, W. T. Asymptotic approximations to crack problems. *Mechanics of Fracture: Method of Analysis and Solutions of Crack Problems*, Ed. Sih G. C., Leyden: Noordhof International Publishing, 1973, pp. 131-178.

[38] VOJTEK, T.; PIPPAN, R.; HOHENWARTER, A.; HOLÁŇ, L.; POKLUDA, J. Near-threshold propagation of mode II and mode III fatigue cracks in ferrite and austenite. *Acta Materialia*, 2013, vol. 61, pp. 4625-4635.

[39] HORNÍKOVÁ, J.; ŠANDERA, P.; POKLUDA, J. Linear-Elastic and Elastoplastic Mode II and III Crack Tip Stress-Strain Fields in Cylindrical Specimens with Circumferential Crack. *Key Engineering Materials*, 2010, vol. 417-418, pp. 321-324, ISSN: 1662-9795.

[40] KLESNIL, M.; LUKÁŠ, P. *Fatigue of Metallic Materials*. Amsterdam: Elsevier, 1992, 270 p.

[41] POOK, L. P. *Crack Paths*. Southampton-Boston: Wit Press, 2002. 154 p. ISBN 978-1-8531-2927-8

[42] VATNE, I. R.; STUKOWSKI, A.; THAULOW, C.; OSTBY, E.; MARIAN, J. Three-dimensional crack initiation mechanisms in bcc-Fe under loading modes I, II and III. *Materials Science and Engineering A*, 2013, vol. 560, pp. 306-331.

[43] OHR, S. M. An electron microscope study of crack tip deformation and its impact on the dislocation theory of fracture. *Materials Science and Engineering*, 1985, vol. 72, pp. 1-35.

[44] LIAW, P. K.; LEA, T. R.; LOGSDON, W. A. Near-threshold fatigue crack growth behavior in metals. *Acta Metallurgica*, 1983, vol. 31, pp. 1581-1587.

[45] POKLUDA, J; PIPPAN, R.; VOJTEK, T.; HOHENWARTER, A. Near-threshold Behaviour of Shear-mode Fatigue Cracks in Metallic Materials. *Fatigue & Fracture of Engineering Materials & Structures*, 2014, vol. 37, pp. 232-254.

[46] PIPPAN, R. Threshold and effective threshold of fatigue crack propagation in ARMCO iron I: The influence of grain size and cold working. *Materials Science and Engineering A*, 1991, vol. 138, pp. 1-13.

[47] IRWING, P. E.; ROBINSON, J. L.; BEEVERS, C. J. Fatigue crack closure in titanium and titanium alloys. *International Journal of Fracture*, 1973, vol. 9, pp. 105-108.

[48] BOYCE, B. L.; RITCHIE, R. O. Effect of load ratio and maximum stress intensity on the fatigue threshold in Ti-6Al-4V. *Engineering Fracture Mechanics*, 2001, vol. 68, pp. 129-147.

[49] POKLUDA, J.; KONDO, Y.; SLÁMEČKA, K.; ŠANDERA, P.; HORNÍKOVÁ, J. Assessment of Extrinsic Crack Tip Shielding in Austenitic Steel near Fatigue Threshold. *Key Engng. Mater.*, 2008, vol. 385-387, pp. 49-52.

AUTHOR'S CV

Name: **Ing. Tomáš Vojtek**
Born: 14th August 1986 in Havířov, Czechoslovakia

Education

2008: Bachelor Degree, Transport Means, University of Pardubice, Czech Republic (Passed with honours)
2010: Master Degree, Transport means, University of Pardubice, Czech Republic (Passed with honours)
Since 2010: Ph.D. studies, Physical and Materials Engineering; Brno University of Technology, Czech Republic

Career

Since 2012: Junior researcher, Institute of Physical Engineering, Faculty of Mechanical Engineering (FME), Brno University of Technology (BUT), Czech Republic (part-time, 0.1)
Since 2013: Junior researcher, Central European Institute Technology (CEITEC), BUT, Czech Republic (part-time, 0.3)

Scientific Field

Materials Science and Engineering: fatigue crack propagation in metallic materials.

Pedagogic Activities

Since 2010: Tuition of laboratory seminar of Physics

Academic Interships Abroad

Since 2010: 10 months at the Erich Schmid Institute of Materials Science, Austrian Academy of Sciences, Leoben, Austria (research: shear-mode fatigue cracks in metals)

Projects

Principal researcher:
2012: Growth threshold conditions and topography of cracks loaded in modes II and III, project of FME BUT
2013: Quantitative fractography of shear fatigue cracks in ARMCO iron and titanium, project of FME BUT

Member of the research team:

2011: Deformation stability of crystals and cracks in solids under multiaxial loading, project of FME BUT

2011 – 2013: Modelling of deformation and damage of solids from nanoscopic level, project of FME BUT

2012 – 2015: Fatigue of NiTiX High Temperature Shape Memory Alloy Actuators /FACT/, project of Czech Science Foundation No. GAP107/12/0800

Activities

Since 2012: Member of the European Structure Intergrity Society (ESIS)

LIST OF AUTHOR'S PUBLICATIONS

Journals:

1. Vojtek T., Pokluda J., Hohenwarter A., Pippan R.: Three-dimensional Morphology of Fracture Surfaces Generated by Modes II and III Fatigue Loading in Ferrite and Austenite. *Engineering Fracture Mechanics* 108 (2013), 285–293.
2. Vojtek T., Pippan R., Hohenwarter A., Holáň L., Pokluda J.: Near-threshold Propagation of Mode II and Mode III Fatigue Cracks in Ferrite and Austenite. *Acta Materialia* 61 (2013), 4625–4635.
3. Vojtek T., Pokluda J.: Experimental Investigation of Modes II and III Fatigue Crack Growth in Unalloyed Titanium. *Key Engineering Materials* (2014) 592–593, 797–800.
4. Pokluda J., Pippan R., Vojtek T., Hohenwarter A.: Near-threshold Behaviour of Shear-mode Fatigue Cracks in Metallic Materials. *Fatigue & Fracture of Engineering Materials & Structures* 37 (2014), 232–254.
5. Vojtek T., Pokluda J., Horníková J., Šandera P.: Description of Fatigue Crack Growth under Modes II, III and II+III in Terms of J-integral. *Procedia Materials Science* (2014), in print.

Conference Proceedings:

1. Vojtek T.: Experiments on Fatigue Crack Propagation in Loading Modes II and III in Metals. In: Náhlík, L.; Zouhar, M.; Ševčík, M.; Seitl, S.; Majer, Z. (Eds.), *13th Conference Applied mechanics 2011*, pp. 239–242, ÚFM AVČR, Brno (2011).
2. Vojtek T., Pokluda J.: Paths of Shear-mode Cracks in Ferritic and Austenitic Steel. In: A. Carpinteri, F. Iacoviello, L.P. Pook, L. Susmel (Eds.), *Crack Paths 12*, pp. 727–734, Gaeta (2012).
3. Vojtek T., Pokluda J., Šandera P., Horníková J., Slámečka K., Hohenwarter A., Pippan R.: Near-threshold Fatigue Crack Propagation under Mixed-mode II+III in ARMCO Iron. In: R. Goldstein (Ed.), *Fracture Mechanics for Durability, Reliability and Safety (ECF19)*, p. 188 - CD ROM, Kazan Scientific Centre of the Russian Academy of Sciences, Kazan (2012).

ABSTRACT

The work is focused on fatigue crack propagation under modes II and III and II + III in the near-threshold region in metallic materials. A special emphasis is given to experimental determination of effective shear-mode thresholds and their comparison with theoretical models of propagation of ideal fatigue cracks. The criterion for mode I branching is also studied in terms of the effective stress intensity factor ranges.

The amount of experimental data available in the literature is limited due to problems related to closure effects of shear-mode cracks, i.e. friction between fracture surfaces. Moreover, the design of pure modes II and III experiment is rather difficult. A significant difference in closure effects of mode II and mode III cracks due to branching to local mode I is emphasized. Under remote mode III loading, factory-roof like morphology is usually generated, while a deflection of mode II cracks along their front line is created.

Experiments were conducted for ARMCO iron, titanium, nickel and austenitic steel on three types of specimens for shear-mode crack loading. A special technique of precrack generation was used which enabled a closure-free loading at the beginning of the shear-mode experiments. For all investigated materials the effective thresholds under the remote mode II loading were found to be about 1.7 times lower than those under the remote mode III. Measured crack growth rates were plotted in terms of the diagrams $\Delta a/\Delta N$ vs. ΔK.

Fracture morphologies were analyzed by stereophotogrammetry in SEM. Tendency to local mode I branching was assessed by a measurement of local deflection and twist angles. The lowest angles of both mode II and mode III cracks where identified for the ARMCO iron, where the cracks propagated in a nearly coplanar manner according to the model of emission of shielding dislocations from the crack tip. In titanium and nickel the mean angles where higher but they did not reach the theoretical angles for local mode I branches. In austenitic steel, both mode II and mode III cracks propagated in highly deflected or twisted planes by local mode I mechanism. It was suggested that the mechanism according to the decohesion model was predominant here and that the differences in the behaviour of these materials can be explained by different numbers of available slip systems in their crystal lattices.

Theoretical considerations based on the crack-growth micromechanism combined with the mean deflection angle enabled to propose an analytical formula for effective thresholds of mode II cracks in a good agreement with experimental results. The mode I branching criterion in terms of effective threshold values leads to a critical deflection angle of $\approx 40°$ that is related to a transition from the local shear to the opening mode. This angle is practically independent of a material.